The anharmonic quartic force field infrared spectra of three polycyclic aromatic hydrocarbons: Naphthalene, anthracene, and tetracene

Cameron J. Mackie' , Alessandra Candian, Xinchuan Huang, Elena Maltseva, Annemieke Petrignani, Jos Oomens, Wybren Jan Buma, Timothy J. Lee, and Alexander G. G. M. Tielens

Citation: The Journal of Chemical Physics **143**, 224314 (2015); doi: 10.1063/1.4936779
View online: http://dx.doi.org/10.1063/1.4936779
View Table of Contents: http://aip.scitation.org/toc/jcp/143/22
Published by the American Institute of Physics

The anharmonic quartic force field infrared spectra of three polycyclic aromatic hydrocarbons: Naphthalene, anthracene, and tetracene

Cameron J. Mackie,[1,a)] Alessandra Candian,[1] Xinchuan Huang,[2] Elena Maltseva,[3] Annemieke Petrignani,[1,4] Jos Oomens,[4] Wybren Jan Buma,[3] Timothy J. Lee,[5] and Alexander G. G. M. Tielens[1]
[1]*Leiden Observatory, Leiden University, P.O. Box 9513, 2300 RA Leiden, The Netherlands*
[2]*SETI Institute, 189 Bernardo Avenue, Suite 100, Mountain View, California 94043, USA*
[3]*University of Amsterdam, Science Park 904, 1098 XH Amsterdam, The Netherlands*
[4]*Radboud University, FELIX Laboratory, Toernooiveld 7, 6525 ED Nijmegen, The Netherlands*
[5]*NASA Ames Research Center, Moffett Field, California 94035-1000, USA*

(Received 25 August 2015; accepted 17 November 2015; published online 10 December 2015)

Current efforts to characterize and study interstellar polycyclic aromatic hydrocarbons (PAHs) rely heavily on theoretically predicted infrared (IR) spectra. Generally, such studies use the scaled harmonic frequencies for band positions and double harmonic approximation for intensities of species, and then compare these calculated spectra with experimental spectra obtained under matrix isolation conditions. High-resolution gas-phase experimental spectroscopic studies have recently revealed that the double harmonic approximation is not sufficient for reliable spectra prediction. In this paper, we present the anharmonic theoretical spectra of three PAHs: naphthalene, anthracene, and tetracene, computed with a locally modified version of the SPECTRO program using Cartesian derivatives transformed from Gaussian 09 normal coordinate force constants. Proper treatments of Fermi resonances lead to an impressive improvement on the agreement between the observed and theoretical spectra, especially in the C–H stretching region. All major IR absorption features in the full-scale matrix-isolated spectra, the high-temperature gas-phase spectra, and the most recent high-resolution gas-phase spectra obtained under supersonically cooled molecular beam conditions in the CH-stretching region are assigned. [http://dx.doi.org/10.1063/1.4936779]

I. INTRODUCTION

Polycyclic aromatic hydrocarbon (PAH) molecules are a family of molecules consisting of two or more fused benzenoid rings with hydrogen atoms capped around the free edges. These molecules are very stable and participate in many reactions, which make them an attractive focus for various physics/chemistry research areas. For example, they serve as model compounds for innovative carbon-based materials, such as nanotubes and graphene;[1–3] their carcinogenic properties make them widely studied pollutants of water, air, and even food;[4] and they are common by-products of both natural and anthropogenic pyrolysis and combustion.[5,6]

While ubiquitous and abundant on the Earth, PAHs are also of special interest to astronomers, as they are potentially responsible for the so-called Aromatic Infrared (IR) Bands (AIBs).[7,8] These bands have been observed in the IR spectrum of a variety of astrophysical environments: from young stellar objects, to planetary and reflection nebulae, to the diffuse interstellar medium, even in the emissions from entire galaxies.[9] PAHs may be formed in outflows of aging stars and their ubiquity and abundance lead to an estimate that PAH molecules lock up 10%-20% of the cosmic carbon and are responsible for 30% of the IR emissions found in galactic observations.[9] Experimentalists and theoreticians have been working hand in hand to study the PAH IR spectroscopy as a means to identify relevant molecular structures and to use them as a tool to characterize the physical and chemical conditions in various astrophysical environments.

Experimental IR spectra have been reported for many PAHs.[10,11,13–18] However due to the involatile nature of PAHs, low-temperature high-resolution spectra (as needed to understand the molecular physics involved in order to compare with astronomical observations) are difficult to produce. Most experimental spectra were acquired using low-temperature matrix-isolation techniques or high-temperature gas-phase spectroscopy. The matrix-isolation spectra (MIS) suffer from the interaction with the matrix environment and are subject to hard to predict changes in line positions, intensities, band profiles, and even band splittings.[19] Likewise, for the high-temperature gas-phase spectra, temperature effects can mask underlying physics and make extrapolations to low temperatures difficult. For example, in a 2009 study by Pirali *et al.*,[20] the room temperature high-resolution rovibrational spectrum of naphthalene was presented, and most of the analysis in which was aimed at understanding the multiple bands in the low energy spectrum region, i.e., 400–900 cm^{-1}, due to temperature effects. Other issues, including contaminations originating from isotopologues and other PAH species, may further complicate the acquired spectra and analysis.

The difficulties in obtaining and understanding the IR spectrum of PAHs have led to an ever-increasing reliance on

a)Electronic mail: mackie@strw.leidenuniv.nl

computational quantum chemistry. Computational chemistry approaches have been used to explain the IR spectrum of large ($N_C \geq 50$), astronomically relevant PAHs. In this context, it is important to note that databases of the theoretical PAH spectra have been created and available online.[21,22] Previous computations were typically performed within the framework of Density Functional Theory (DFT), employing the B3LYP functional with a small basis set (e.g., 4–31G). The double harmonic approximation is used for vibrational IR intensities. A scaling factor is used to down-scale the calculated harmonic frequencies to match with matrix-isolation experimental features.[23] As a first-order approximation, this approach has been successful enough in reproducing the overall IR spectrum of certain individual PAHs roughly, but serious problems persist when comparing it with high-resolution experiments. Specifically, the IR features in the C–H stretching region are poorly modeled using the harmonic level analysis, which include scaled harmonic frequencies and double harmonic intensities. This is most likely due to phenomena such as mode couplings and resonances that are not described at the harmonic level.

The most recent Gaussian 09[24,25] release contains an improved module for second-order vibrational perturbations theory (VPT2) anharmonic analysis of molecules, thus enabling a regular (or standard) VPT2-based IR spectrum simulation of PAHs. In this work, we make use of this module and enhance its VPT2 analysis by additional treatments on vibrational state resonances, as will be described below. The anharmonic IR spectra of the three smallest linear PAHs, naphthalene ($C_{10}H_8$), anthracene ($C_{14}H_{10}$), and tetracene ($C_{18}H_{12}$) (see Fig. 1) are computed and compared with the currently available low resolution high-temperature gas-phase[16] (NIST), and argon MIS[11]. Moreover, we present low-temperature high-resolution gas-phase experimental IR absorption spectra of the three PAHs (first presented in an astrophysical companion paper to this work[26]), which allows for the most direct comparison with theory possible and thus provides validation for our approach.

The article is built up in the following way. Section II briefly describes the theory behind the anharmonic calculations. Section III A provides a description of the computational methods and programs that are used to perform the theoretical calculations. Section III B describes the experimental methods for producing the gas-phase IR absorption spectra in the CH–stretching region. The results are arranged into two subsections: a comparison of the full anharmonic IR spectra with NIST and MIS data (Section IV A), and an in-depth comparison of the calculated CH-stretching region with low-temperature high-resolution gas-phase experimental spectra (Section IV B). Three subsections are presented in Sec. V : Sections V A, V B, for IV A and IV B, respectively, plus Section V C for astrophysical implications. The Conclusions follow at the end.

II. THEORY

Theoretical predictions of the vibrational IR spectrum of molecules are most often performed at the harmonic level. If the geometry of a stationary point of a molecule is known,

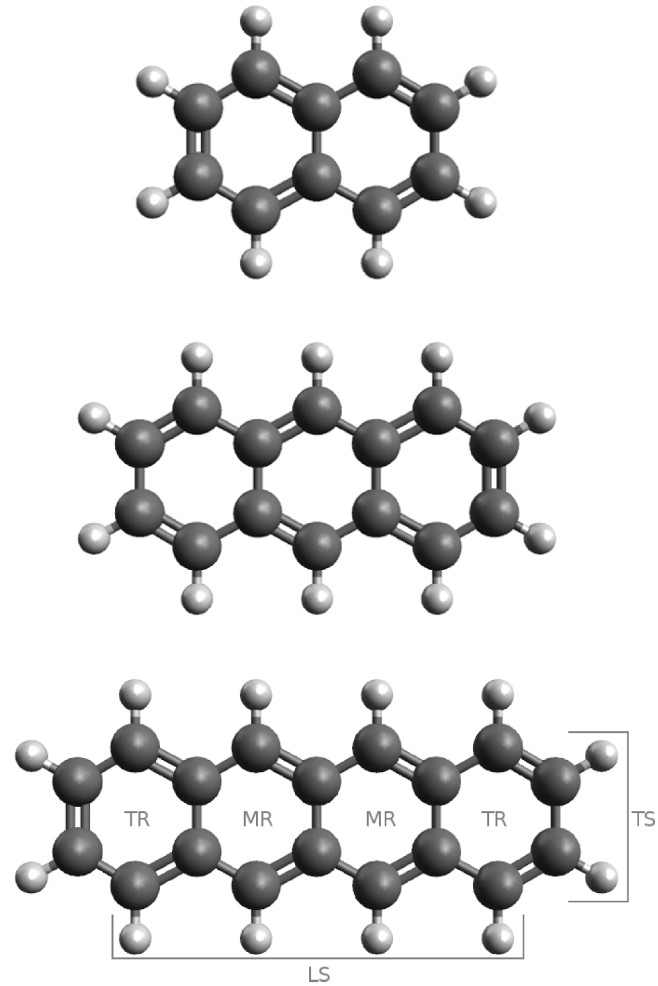

FIG. 1. From top to bottom: naphthalene, anthracene, and tetracene. The rings are designated as either terminal ring (TR) or middle ring (MR). The side CH groups are designated as either terminal side CH groups (TS) or long side CH groups (LS). The designations are used for the vibrational mode descriptions in Appendix.

then the vibrational potential can be approximated as a simple pairwise interaction between atoms, akin to Hooke's law (see Ref. 27 for a complete description),

$$V = \frac{1}{2}\sum_{i=1}^{3N}\sum_{j=1}^{i} F_{ij}X_iX_j, \tag{1}$$

where V is the total vibrational potential, $F_{ij} = \frac{\partial V}{\partial X_i \partial X_j}$ are the quadratic force constants (spring constant k_{ij} in Hooke's Law) between atoms i and j, and X_i and X_j are the Cartesian coordinates of atom i and j relative to the stationary point.

Ab initio calculations can generate these force constants using various methods (see Ref. 28 for an overview). Once these force constants are known, a mass-weighted Hessian matrix $\mathbf{H}$ can be built where each $(i, j)th$ entry of the matrix is generated by dividing the corresponding force constant F_{ij} by the square root of the product of the masses of atom i and j ($\sqrt{m_i m_j}$). This matrix is then diagonalized to produce a set of eigenvectors defining the vibrational normal modes at the stationary point; the corresponding eigenvalues give the harmonic frequencies (or energies) of the corresponding vibrational normal modes (see Ref. 27 for a full review). This method, while simple, is not a realistic model for the potential energy surface and overlooks anything beyond harmonic level, e.g., vibrational anharmonicities, and mode couplings and resonances, which can significantly affect the spectra, especially true for those systems with many vibrational resonances such as PAH molecules.

To account for these effects, an improved expression for the vibrational potential energy surface is needed. The harmonic potential (Eq. (1)) can then be thought of as the first non-zero term in a Taylor expansion of the vibrational potential energy function. The full vibrational potential surface would be the Taylor expansion to infinite order around the stationary point (equilibrium geometry) of the molecule. For the purpose of this work, the first three non-zero terms of the Taylor expansion are considered relevant,[28]

$$\begin{aligned} V = V_0 &+ \sum_{i=1}^{3N} \left(\frac{\partial V}{\partial X_i}\right)_{V_0} X_i \\ &+ \frac{1}{2}\sum_{i=1}^{3N}\sum_{j=1}^{i} \left(\frac{\partial^2 V}{\partial X_i \partial X_j}\right)_{V_0} X_i X_j \\ &+ \frac{1}{6}\sum_{i=1}^{3N}\sum_{j=1}^{i}\sum_{k=1}^{j} \left(\frac{\partial^3 V}{\partial X_i \partial X_j \partial X_k}\right)_{V_0} X_i X_j X_k \\ &+ \frac{1}{24}\sum_{i=1}^{3N}\sum_{j=1}^{i}\sum_{k=1}^{j}\sum_{l=1}^{k} \left(\frac{\partial^4 V}{\partial X_i \partial X_j \partial X_k \partial X_l}\right)_{V_0} X_i X_j X_k X_l. \quad (2) \end{aligned}$$

Since V_0 is arbitrary and set to zero, and the first derivative terms are zero at a stationary point; this leaves the terms containing the second, third, and fourth derivatives. These non-zero derivatives are referred to as the quadratic, cubic, and quartic force constants, respectively. Collectively this group of force constants for a given molecule is referred to as the quartic force field (QFF). Given the equilibrium geometry, the QFF of a molecule can be calculated analytically or numerically through small displacements of the atoms along a defined set of coordinates. In the VPT2 anharmonic vibrational analysis, the quadratic force constants are used to obtain the harmonic solution (as described above) which is then corrected by a second-order perturbation using the cubic and quartic force constants. Following Ref. 29, the energy of the perturbed states (for an asymmetric top) are given by

$$E(\nu) = \sum_k \omega_k \left(\nu_k + \frac{1}{2}\right) + \sum_{k\le l} x_{kl} \left(\nu_k + \frac{1}{2}\right)\left(\nu_l + \frac{1}{2}\right), \quad (3)$$

where the anharmonic constants are given by

$$x_{kk} = \frac{1}{16}\phi_{kkkk} - \frac{1}{16}\sum_m (\phi_{kkm})^2 \left[\frac{8\omega_k^2 - 3\omega_m^2}{\omega_m\left(4\omega_k^2 - \omega_m^2\right)}\right], \quad (4)$$

$$\begin{aligned} x_{kl} = \frac{1}{4}\phi_{kkll} &- \sum_m \frac{\phi_{kkm}\phi_{llm}}{4\omega_m} \\ &- \sum_m \frac{(\phi_{klm})^2 \omega_m \left(\omega_k^2 + \omega_l^2 - \omega_m^2\right)}{2\Omega_{klm}} \\ &+ \sum_\alpha B_\alpha^e (\zeta_{kl}^\alpha)^2 \left[\frac{\omega_k}{\omega_l} + \frac{\omega_l}{\omega_k}\right], \quad (5) \end{aligned}$$

$$\begin{aligned} \Omega_{klm} = &(\omega_k + \omega_l + \omega_m)(-\omega_k + \omega_l + \omega_m) \\ &\times (\omega_k - \omega_l + \omega_m)(\omega_k + \omega_l - \omega_m), \quad (6) \end{aligned}$$

$$B_\alpha^e = \frac{h}{8\pi^2 c I_\alpha^e}, \quad (7)$$

where ϕ_{xxx} and ϕ_{xxxx} are the cubic and quartic force constants, respectively, ω are the harmonic frequencies, ν are the vibrational fundamental states, ζ_{kl}^α are the Coriolis coupling constants, and I_α^e are the moments of inertia.

The standard VPT2 method still contains caveats such as the singularities, so-called *resonances*, that occur when a set of harmonic frequencies or their sums, differences, or combinations are accidentally nearly equal and of the same symmetry (see Ref. 30 for a detailed explanation). Normally, there are two main types of vibrational resonances considered in a VPT2 anharmonic analysis: a type-one Fermi resonance, where a first overtone state is approximately equal to a vibrational fundamental state ($\nu_i \approx 2\nu_j$), and a type-two Fermi resonance, where a combination state is approximately equal to a fundamental ($\nu_i \approx \nu_j + \nu_k$). There also exists additional types of resonances that become important when considering ro-vibrational spectra, e.g., Darling–Dennison resonances, where two first overtones are approximately equal ($2\nu_i \approx 2\nu_j$), and Coriolis resonances where two fundamentals are approximately equal ($\nu_i \approx \nu_j$).[31] Typically, the effect of a resonance is that the higher energy state in the resonance pair tends to be pushed to even higher energies and the lower energy state to even lower energies and also intensity can be transferred from one state to the other. These effects can significantly alter the band positions, the number of bands, and overall intensities in the IR spectrum. To properly treat such resonant states, related terms need to be removed from the VPT2 treatment and handled separately with a method akin to degenerate second-order perturbation theory as described in Refs. 31 and 30. If a given mode is simultaneously involved in more than one resonance (as happens for PAH molecules), all the modes (and overtones and combination-bands) involved need to be treated together as a group referred to as a *polyad*. (see Ref. 30 for a complete description). For a specific vibrational resonance polyad, a matrix is constructed using the appropriate anharmonic constants (as given in Ref. 31) and diagonalized. The resulting eigenvalues are then the new line positions of the involved states and the eigenvectors (squared) represent the complexity of state mixings. While we use a variational polyad approach to correct for resonant states in VPT2, an alternative approach is vibrational quasi-degenerate perturbation theory (VQDPT2)[32,33] which has shown some success as well.

Vibrational IR intensities can also be either harmonically or anharmonically computed. So-called double harmonic intensities of vibrational modes are calculated using the derivative of the dipole moment with respect to a normal coordinate. By definition, at the harmonic level, combination-bands and overtones have zero IR intensity. However, when considered anharmonically, these combination-bands and overtones can be IR-active and have significant intensity. The anharmonic treatment of these intensities has been described previously in Refs. 34 and 35. Perhaps more importantly, IR intensity can be redistributed due to resonances

TABLE I. Percentage of mixing between resonance-affected states in the b_{1u} symmetry polyad of naphthalene in the CH-stretching region, which was used to estimate the IR intensity sharing across the polyad. See text for details.

Mode	2946	2956	2968	2979	3029	3066	3081	3142	3176
ν_3	9.0	0.7	1.6	2.4	0.1	81.3	2.8	0.0	2.2
ν_7	3.7	8.9	0.2	5.7	51.6	1.4	24.6	3.8	0.1
$\nu_{10}+\nu_{11}$	0.3	0.0	0.0	0.1	0.2	1.8	0.1	0.2	97.4
$\nu_{10}+\nu_{13}$	0.0	1.6	0.1	1.2	26.1	1.3	69.3	0.2	0.1
$\nu_{12}+\nu_{14}$	35.2	0.1	46.6	9.2	2.6	6.1	0.1	0.0	0.0
$\nu_{11}+\nu_{15}$	25.8	36.9	20.4	8.4	6.6	1.4	0.4	0.0	0.0
$\nu_{10}+\nu_{16}$	20.1	38.7	28.7	11.9	0.0	0.6	0.0	0.0	0.0
$\nu_9+\nu_{17}$	5.8	13.0	2.3	61.0	11.2	6.0	0.6	0.0	0.0
$\nu_9+\nu_{12}$	0.1	0.2	0.0	0.1	1.6	0.1	2.0	95.8	0.2

between fundamentals and combination and overtone bands as well. Intensity redistribution due to Fermi resonances and anharmonicity has been addressed by Vázquez and Stanton within the context of VPT2.[36] In the present work, we have adopted a similar but simpler approach. That is, we have used the eigenvectors of the polyad matrix to distribute IR intensity across the polyad in conjunction with the double harmonic IR intensities of the fundamental vibrational frequencies.

In the present work, we have redistributed the IR intensity across a polyad by using the eigenvectors of the polyad matrix together with the double harmonic IR intensities of the fundamentals involved in the polyad. We used the double harmonic intensities, because it was found that the Gaussian09 anharmonic IR intensities for a fundamental involved in a polyad resonance often blew up, which we surmise due to resonant terms that need to be removed, as described by Vázquez and Stanton.[36] Table I gives an example for the IR-active b_{1u} polyad involving the naphthalene CH-stretching fundamentals to illustrate how the intensity borrowing is calculated. The first column lists all the states in the polyad, while the remaining column headers are the eigenvalues (or state energies, in cm^{-1}) diagonalized from the polyad matrix. The elements of these columns are the squared eigenvectors and represent the percentage contribution of each polyad state. Accordingly, the vibrational intensity of a diagonalized state can be estimated as the dot product of the related squared eigenvector and a vector of original contributing state intensities. For example, the state at 2946 cm^{-1} borrows 9.0% of the intensity of the original ν_3 vibrational state, 3.7% of the intensity of the original ν_7 vibrational state, and 0.3% of the intensity of the original $\nu_{10} + \nu_{11}$ combination band. See Sec. III A for more details of the intensities adopted for each original states.

III. METHODS

A. Theoretical methods

Quantum chemistry calculations were performed in two stages, with two separate software packages: Gaussian 09[24] and SPECTRO.[37] Gaussian 09 was used to compute the optimized geometries, harmonic vibrational spectra, as well as the quadratic, cubic and quartic normal coordinate force constants within the DFT framework, using the B971 functional[38] and the T2ZP basis[39] for each molecule. In these calculations, a tight convergence criterion was used for the geometry optimization and a very fine grid (Int = 200 974) for numerical integrations, following the suggestions in Refs. 40 and 41.

Although the latest release of Gaussian 09 (D.01) can also output the VPT2-based anharmonic spectrum of a molecule,[24] we have found that these spectra cannot reproduce the IR features observed in the CH-stretching region of PAHs.[26] We believe this is mainly due to polyads not being used to determine intensity sharing between resonant modes[34] though we do not know for sure since we do not have access to the source code. Actually, the resonance and intensity borrowing effect seems to be minor when the computational results are compared with low-resolution gas-phase spectra,[42] but this is not the case for low-temperature high-resolution gas-phase spectra with significant resonances such as the PAHs C-H stretches. Therefore, the VPT2 treatment was carried out by the second program SPECTRO. SPECTRO allows for resonances to be handled in polyads which then are used to redistribute the intensities across the resonant modes (vide infra). This approach, while approximate, does avoid the difficulty of dealing directly with the singularities that occur in resonant calculations of intensities. If not involved in resonances or polyads, we have found the anharmonic combination or overtone band intensities computed by Gaussian G09 to be reliable and have used these.

The optimized molecular minimum structure and the force constants calculated by Gaussian 09 is used as input for SPECTRO. Since Gaussian evaluates the QFF along the normal modes of a molecule, the QFF force constants are represented in a normal coordinate basis. The current version of SPECTRO can take either Cartesian derivatives or internal coordinate force constants as input, but not a normal coordinate QFF. As such, a linear transformation method from a normal coordinate QFF to a Cartesian coordinate QFF was developed and implemented to mesh the two software packages together.[43]

Two SPECTRO threshold parameters control the number of states to be included in a resonance: (a) the maximum energy separation of the states (Δ) (i.e., the denominator in resonant terms), and (b) the minimum magnitude of the interaction strength between states (W) (i.e., the numerator in resonant terms). In the present study, the SPECTRO default values of Δ = 200 cm^{-1} and W = 10 cm^{-1} were used, respectively. Testing with larger thresholds showed no significant changes in the resulting spectra.

The final anharmonic spectrum of each target molecule is therefore constructed using the following: (a) all line positions (fundamentals, overtones, combination-bands, resonances, and polyads) as determined using SPECTRO and (b) three types of intensities, i.e., one for vibrational fundamentals, one for combination-bands/overtones not involved in resonances, and one for those involved in resonances/polyads. It should be noted that for those states potentially affected by resonances, we found that the double harmonic intensities were more reliable than Gaussian's anharmonic intensities. Therefore, the anharmonic intensities from Gaussian 09 are only used for the combination-bands/overtones that have zero intensity in the double harmonic approximation and cannot borrow intensity from resonances/polyads. The double harmonic intensities are used for all other states, including non-resonant fundamentals. For the resonances/polyads, the double harmonic intensities are used in the intensity sharing across the modes of the polyad using the squared eigenvectors from the polyad treatment as described earlier in Section II.

B. Experimental methods

A supersonic pulsed source similar to Ref. 44 was used to record the low-temperature high-resolution gas-phase spectra in the CH stretching region (see also the companion paper Ref. 26). The samples were heated in an oven and then supersonically cooled with a typical pulse duration of 190 μs and argon at a backing pressure of 2.2 bars as a buffer gas. The molecular beam was then introduced into the ionization chamber through a 2 mm diameter skimmer where they were ionized using a Resonance Enhanced MultiPhoton Ionization (REMPI) scheme. The ions created were accelerated into a reflector time-of-flight tube and detected with a dual microchannel plate detector (Jordan Co.), yielding mass spectra with a resolution of $M/\Delta M$ of about 2000.

IR absorption spectra have been recorded using an IR–UV depletion scheme. In these experiments, a constant ion signal was created using a two-color ionization scheme in which a frequency-doubled dye laser (Sirah Cobra Stretch) pumped by a 30 Hz Nd:Ya$_g$ laser (Spectra Physics Lab 190) excites molecules to the first excited state. From this state, the molecules were ionized by an ArF excimer laser (Neweks PSX-501), which is in temporal overlap with the dye laser output. To record the IR absorption, these two laser beams were preceded by an IR laser beam with a linewidth of 0.07 cm^{-1}, which produces a dip in the ion signal upon IR absorption of the molecules under investigation. The IR beam was generated by difference frequency mixing of the fundamental output of a LDS 798 dye laser (Sirah Precision Scan) pumped by a 30 Hz Nd:Ya$_g$ laser (Spectra Physics Lab 190) with the fundamental of the Nd:Ya$_g$ laser.

In these double-resonance experiments, overlap of the two laser beams and matching their size are crucial for obtaining the optimal depletion of the ground state. The IR beam has therefore been focused slightly with a long-focus lens beam with its focus after the molecular beam. Similarly, special care has been taken to record spectra under non-saturating conditions. Experimentally, it has been found that in these experiments depletion is optimal for a time delay between the two laser beams of 200 ns.

IV. RESULTS

A. Full infrared range

The full vibrational IR spectra of naphthalene, anthracene, and tetracene are presented in Figures 2–4. A comparison is given between the experimental spectra (NIST cq. MIS, bottom panel) and two theoretical spectra: anharmonic (this work, middle panel) and harmonic (this work, top panel). The harmonic spectra were calculated with Gaussian 09 using the same functional and basis set as in the anharmonic case. The experimental data for naphthalene and anthracene in these plots are taken from the NIST database[16] (gas-phase, T = 300 K). The experimental data for tetracene are an argon matrix-isolation spectrum taken from Ref. 11. Some water contamination is present in the tetracene experimental data, and it has been greyed out in the figure. Each of the three comparisons also includes an inset that shows the 1000–3000 cm^{-1} region magnified in order to show detail. The choice for these three experimental spectra was based on the availability of data for the widest vibrational IR range. Original gas-phase or uncontaminated matrix-isolation data are not available for tetracene, so the spectrum was produced by combining four figures from Ref. 11.

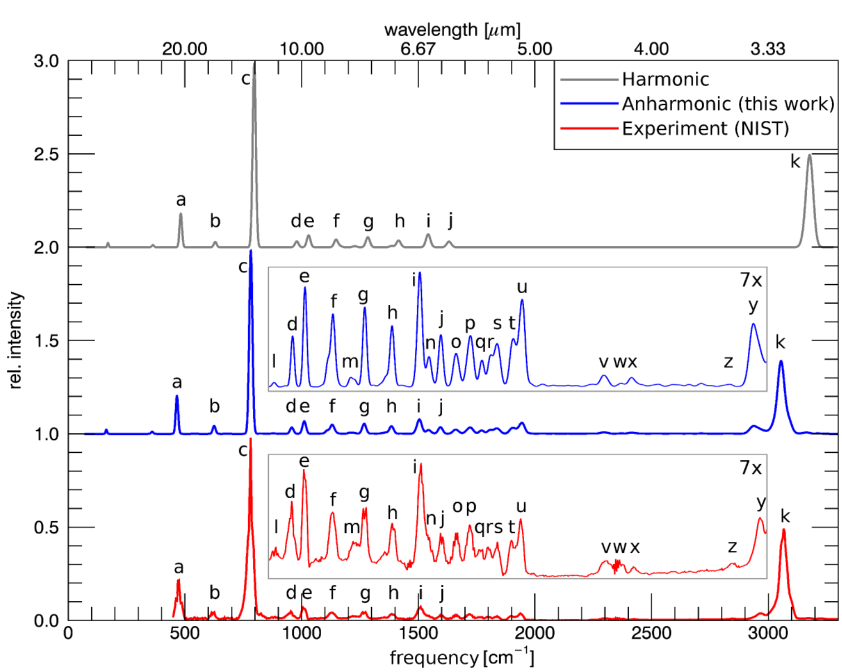

FIG. 2. Full IR spectrum of naphthalene calculated using two methods, harmonic (top) and anharmonic (this work) (middle), compared with gas-phase spectra at 300 K[16] (bottom). A selected region is shown with the relative intensities increased by a factor of seven (see Section V A for details).

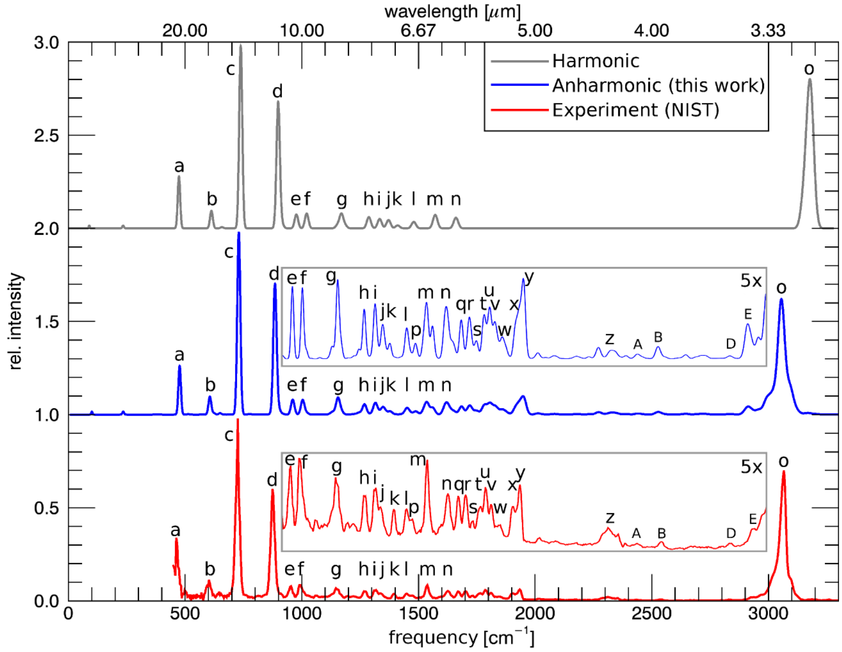

FIG. 3. Full IR spectrum of anthracene calculated using two methods, harmonic (top) and anharmonic (this work) (middle), compared with gas-phase spectra at 300 K[16] (bottom). A selected region is shown with the relative intensities increased by a factor of five (see Section V A for details).

The theoretical overview spectra of naphthalene and anthracene are convolved with a Gaussian profile (FWHM = 18 cm^{-1}) to approximately match the resolution of the experimental gas-phase data. Likewise, the theoretical overview spectrum of tetracene is convolved with a Gaussian profile (FWHM = 3 cm^{-1}) to match the matrix-isolation data. Theoretical frequencies have not been scaled.

Three tables (II, III, and IV) are presented along with these overview spectra. These tables contain the line positions and relative intensities of the experimental data, the harmonic theoretical data, and the anharmonic theoretical data from this work. Since the full IR experimental spectra contain many unresolved features, assignments are based on the convolved theoretical spectrum. The underlying states and combination-bands of the experimental features are determined using the theoretical results. The symmetries of the corresponding bands are also given. The spectroscopic features identified for naphthalene and anthracene are based on the excellent correspondence between experiment and theory. The features identified for tetracene are based on the line positions given in Ref. 11. Each feature is identified by a letter that corresponds to the letters appearing in the corresponding Figures 2–4. Supplementary material[12] contains the full IR line list, as well as the corresponding polyads for each of the three PAHs. Appendix also provides vibrational mode descriptions for all the vibrational modes included in these tables (Tables VIII–X).

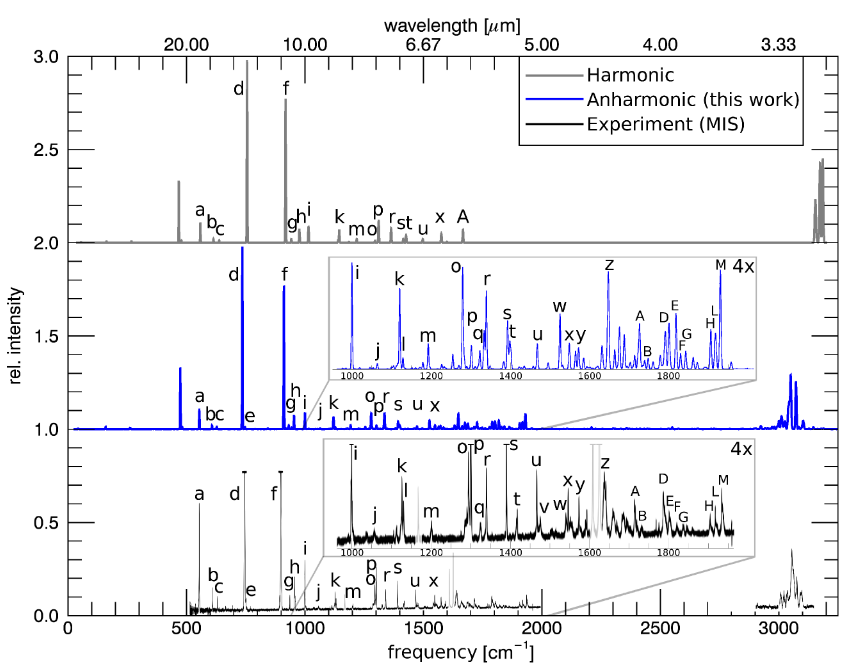

FIG. 4. Full IR spectrum of tetracene calculated using two methods, harmonic (top) and anharmonic (this work) (middle), compared with Ar matrix-isolation spectrum[11] T ≈ 10 K (bottom). A selected region is shown with the relative intensities increased by a factor of four (see Section V A for details). The greyed out lines in the matrix-isolation spectrum are water contamination.

TABLE II. Gas-phase experimental,[16] theoretical harmonic, and theoretical anharmonic (this work) line positions (cm^{-1}), with the corresponding relative intensities and band assignments of the IR features of naphthalene taken from the data used to construct Figure 2. Lines with more than one mode assigned are unresolved in experiment.

ID	Modes	sym	exp	rel. I	harm	rel. I	anharm	rel. I
a	ν_{43}	b_{3u}	474	0.2	482	0.2	465.8	0.2
b	ν_{40}	b_{2u}	620	0.04	630	0.03	625.1	0.03
c	ν_{35}	b_{3u}	782	1	797	1	782.3	1
d	ν_{29}	b_{3u}	950	0.05	979	0.03	958.0	0.03
e	ν_{26}	b_{2u}	1011	0.07	1030	0.07	1011.3	0.07
f	ν_{24}	b_{1u}	1130	0.04	1147.1	0.04	1130.5	0.05
	$\nu_{47}+\nu_{30}$	b_{1u}						
g	ν_{18}	b_{1u}	1269	0.05	1284	0.06	1268.1	0.06
h	ν_{15}	b_{1u}	1388	0.04	1416	0.04	1385.3	0.04
i	ν_{12}	b_{2u}	1511	0.07	1542	0.07	1505.8	0.07
j	ν_{10}	b_{1u}	1599	0.03	1632	0.03	1594.9	0.03
k	See Table V	…	3064	0.5	3176	0.51	3055	0.398
l	$\nu_{47}+\nu_{38}$	b_{1u}	880	0.02	…	…	877	0.003
m	ν_{20}	b_{2u}	1228	0.02	…	…	1212	0.007
	$\nu_{43}+\nu_{36}$	b_{1u}						
n	$\nu_{38}+\nu_{33}$	b_{1u}	1537	0.02	…	…	1544	0.02
o	$\nu_{35}+\nu_{32}$	b_{1u}	1662	0.03	…	…	1661	0.02
	$\nu_{38}+\nu_{29}$	b_{2u}						
p	$\nu_{33}+\nu_{32}$	b_{2u}	1719	0.03	…	…	1722	0.04
	$\nu_{35}+\nu_{30}$	b_{2u}						
	$\nu_{36}+\nu_{28}$	b_{2u}						
q	$\nu_{33}+\nu_{30}$	b_{1u}	1764	0.02	…	…	1772	0.02
r	$\nu_{33}+\nu_{27}$	b_{2u}	1801	0.02	…	…	1810	0.02
s	$\nu_{32}+\nu_{29}$	b_{1u}	1837	0.02	…	…	1836	0.03
	$\nu_{32}+\nu_{28}$	b_{2u}						
t	$\nu_{30}+\nu_{29}$	b_{2u}	1899	0.02	…	…	1905	0.03
	$\nu_{30}+\nu_{28}$	b_{1u}						
u	$\nu_{29}+\nu_{27}$	b_{1u}	1938	0.04	…	…	1944	0.06
	$\nu_{28}+\nu_{27}$	b_{2u}						
v	$\nu_{24}+\nu_{22}$	b_{2u}	2302	0.01	…	…	2295	0.009
	$\nu_{25}+\nu_{18}$	b_{1u}						
	$\nu_{23}+\nu_{22}$	b_{1u}						
	$\nu_{24}+\nu_{21}$	b_{1u}						
w	$\nu_{21}+\nu_{20}$	b_{2u}	2359	0.01	…	…	2368	0.003
x	$\nu_{25}+\nu_{15}$	b_{1u}	2422	0.007	…	…	2414	0.007
	$\nu_{34}+\nu_{9}$	b_{2u}						
	$\nu_{21}+\nu_{18}$	b_{1u}						
z	$\nu_{15}+\nu_{13}$	b_{1u}	2848	0.009	…	…	2835	0.002
	$\nu_{18}+\nu_{11}$	b_{1u}						
y	See Table V	…	2966	0.04	…	…	2938	0.05

B. CH-stretching region

We focus on the CH-stretching region since harmonic level analysis failed to explain the features in this region and significant anharmonic effects are expected. Figures 5–7 compare the anharmonic theoretical lines (top panel) convolved with a FWHM = 1 cm^{-1} Gaussian profile for naphthalene, anthracene, and tetracene, respectively, with our low-temperature high-resolution gas-phase IR absorption experimental spectra (bottom panel). Theoretical frequencies have not been scaled.

Similar to the full IR range, three tables accompany these spectra (Tables V–VII). The assignments are based upon relative intensities, distance between neighbouring bands, and general trends in the shape of the spectrum. In the case

TABLE III. Gas-phase experimental,[16] theoretical harmonic, and theoretical anharmonic (this work) line positions (cm^{-1}), with the corresponding relative intensities and band assignments of the IR features of anthracene taken from data used to construct Figure 3. Lines with more than one mode assigned are unresolved in experiment.

ID	Modes	sym	exp	rel. I	harm	rel. I	anharm	rel. I
a	ν_{58}	b_{3u}	463	0.4	474	0.3	476	0.3
b	ν_{53}	b_{2u}	600	0.1	613	0.1	604	0.1
c	ν_{50}	b_{3u}	726	1	737	1	730	1
d	ν_{42}	b_{3u}	874	0.6	899	0.7	885	0.7
e	ν_{37}	b_{3u}	952	0.08	976	0.08	961	0.08
f	ν_{34}	b_{2u}	991	0.09	1021	0.08	1004	0.08
g	ν_{30}	b_{1u}	1150	0.07	1170	0.08	1154	0.08
h	ν_{25}	b_{1u}	1271	0.06	1287	0.06	1269	0.06
	$\nu_{58}+\nu_{46}$	b_{1u}						
i	ν_{23}	b_{1u}	1314	0.06	1334	0.05	1314	0.05
j	ν_{22}	b_{2u}	1338	0.04	1372	0.05	1347	0.05
	$\nu_{57}+\nu_{42}$	b_{2u}						
k	ν_{21}	b_{2u}	1394	0.04	1412	0.02	1379	0.02
	$\nu_{58}+\nu_{41}$	b_{1u}						
l	ν_{18}	b_{2u}	1448	0.05	1481	0.04	1451	0.040
	ν_{17}	b_{1u}						
m	ν_{15}	b_{2u}	1536	0.09	1572	0.08	1529	0.08
	$\nu_{49}+\nu_{46}$	b_{2u}						
	$\nu_{59}+\nu_{31}$	b_{2u}						
n	ν_{11}	b_{1u}	1626	0.06	1661	0.06	1619	0.07
	$\nu_{47}+\nu_{43}$	b_{1u}						
	$\nu_{47}+\nu_{42}$	b_{2u}						
o	See Table VI		3066	0.7	3176	0.8	3055	0.6
p	$\nu_{50}+\nu_{47}$	b_{2u}	1473	0.03	…	…	1486	0.02
q	$\nu_{44}+\nu_{43}$	b_{2u}	1670	0.05	…	…	1684	0.05
	$\nu_{50}+\nu_{38}$	b_{2u}						
r	$\nu_{44}+\nu_{42}$	b_{1u}	1702	0.06	…	…	1718	0.05
	$\nu_{47}+\nu_{37}$	b_{2u}						
	$\nu_{49}+\nu_{35}$	b_{2u}						
s	$\nu_{46}+\nu_{36}$	b_{2u}	1731	0.03	…	…	1747	0.02
	$\nu_{43}+\nu_{41}$	b_{2u}						
t	$\nu_{42}+\nu_{41}$	b_{1u}	1766	0.04	…	…	1783	0.06
	$\nu_{44}+\nu_{37}$	b_{1u}						
u	$\nu_{44}+\nu_{36}$	b_{2u}	1787	0.06	…	…	1805	0.07
	$\nu_{43}+\nu_{38}$	b_{1u}						
v	$\nu_{43}+\nu_{35}$	b_{2u}	1812	0.05	…	…	1828	0.05
	$\nu_{42}+\nu_{38}$	b_{2u}						
w	$\nu_{41}+\nu_{37}$	b_{1u}	1848	0.03	…	…	1861	0.03
	$\nu_{41}+\nu_{36}$	b_{2u}						
x	$\nu_{38}+\nu_{37}$	b_{2u}	1904	0.04	…	…	…	…
	$\nu_{38}+\nu_{36}$	b_{1u}						
	$\nu_{37}+\nu_{35}$	b_{1u}						
y	$\nu_{36}+\nu_{35}$	b_{2u}	1935	0.07	…	…	1949	0.1
z	$\nu_{51}+\nu_{12}$	b_{2u}	2310	0.02	…	…	2327	0.02
	$\nu_{31}+\nu_{28}$	b_{2u}						
	$\nu_{31}+\nu_{27}$	b_{1u}						
	$\nu_{30}+\nu_{28}$	b_{1u}						
A	$\nu_{29}+\nu_{24}$	b_{1u}	2438	0.008	…	…	2438	0.009
	$\nu_{28}+\nu_{25}$	b_{1u}						
B	$\nu_{40}+\nu_{12}$	b_{2u}	2537	0.01	…	…	2528	0.02
	$\nu_{39}+\nu_{11}$	b_{2u}						
D	$\nu_{19}+\nu_{18}$	b_{2u}	2833	0.01	…	…	2835	0.007
E	See Table VI	…	2932	0.02	…	…	2914	0.05

TABLE IV. Matrix-isolation experimental,[11] theoretical harmonic, and theoretical anharmonic (this work) line positions (cm^{-1}), with the corresponding relative intensities and band assignments of the IR features of tetracene taken from data used to construct Figure 4. Lines with more than one mode assigned are unresolved in experiment.

ID	Modes	sym	exp	rel. I	harm	rel. I	anharm	rel. I
a	ν_{68}	b_{2u}	551.6	0.1	558.7	0.1	554	0.1
b	ν_{66}	b_{1u}	607.7	0.02	613.8	0.02	608	0.02
c	ν_{64}	b_{2u}	627.7	0.01	638.6	0.01	628	0.02
d	ν_{60}	b_{3u}	742.9	1	755.8	1	736	1
e	ν_{61}	b_{2u}	766.7	0.01	754.3	0.01	747	0.01
f	ν_{48}	b_{3u}	895.3	0.8	918.3	0.8	911	0.8
g	ν_{47}	b_{1u}	933.4	0.02	942.4	0.02	932	0.02
h	ν_{45}	b_{3u}	953.6	0.08	...	...	954	0.1
i	ν_{42}	b_{2u}	997.7	0.07	...	...	999	0.1
j	$\nu_{77}+\nu_{63}$	b_{2u}	1054.3	0.01			1064	0.005
k	ν_{39}	b_{1u}	1124.4	0.06	...	...	1120	0.07
l	ν_{40}	b_{2u}	1128.7	0.06	...	...	1129	0.01
m	ν_{34}	b_{1u}	1199.3	0.01	...	...	1193	0.02
o	ν_{29}	b_{1u}	1292.3	0.04	...	...	1279	0.09
p[a]	ν_{29}	b_{1u}	1298.8	0.08	...	...	1301	0.02
	$\nu_{71}+\nu_{57}$							
	$\nu_{73}+\nu_{57}$							
q	$\nu_{69}+\nu_{55}$	b_{2u}	1322.9	0.02	...	...	1323	0.02
r	ν_{27}	b_{2u}	1337.9	0.05	...	...	1339	0.07
s	ν_{23}	b_{2u}	1388.7	0.04	...	...	1393	0.04
t	ν_{25}	b_{1u}	1416.1	0.02	...	...	1399	0.03
u	ν_{20}	b_{2u}	1465.2	0.04	...	...	1469	0.03
v	...	...	1474.1	0.01	...	...	...	...
w	ν_{17}	b_{2u}	1540.1	0.01	...	...	1525	0.05
x	$\nu_{62}+\nu_{55}$	b_{1u}	1546.2	0.02	1575.6	0.05	1549	0.05
y	$\nu_{60}+\nu_{54}$	b_{1u}	1573.2	0.03	...	...	1572	0.02
z	ν_{13}	b_{1u}	1685.5	0.03	1666.7	0.07	1645.7	0.06
A	$\nu_{52}+\nu_{51}$	b_{1u}	1712.7	0.05	...	...	1726	0.04
B	$\nu_{54}+\nu_{48}$	b_{1u}	1730.9	0.01	...	...	1748	0.01
D	$\nu_{54}+\nu_{45}$	b_{1u}	1786.0	0.08	...	...	1791	0.03
E	$\nu_{49}+\nu_{48}$	b_{1u}	1800.3	0.03	...	...	1818	0.05
F	$\nu_{51}+\nu_{46}$	b_{1u}	1819.8	0.01	...	...	1830	0.02
G	$\nu_{51}+\nu_{43}$	b_{2u}	1836.3	0.01	...	...	1842	0.02
H	$\nu_{46}+\nu_{45}$	b_{2u}	1904.2	0.02	...	...	1906	0.04
L	$\nu_{46}+\nu_{44}$	b_{1u}	1917.1	0.02	...	...	1918	0.04
M	$\nu_{44}+\nu_{43}$	b_{2u}	1933.3	0.05	...	...	1931	0.09

[a]Resonance.

of naphthalene, fits of the rotational contours of bands in the experimental spectrum allowed us to determine their symmetries (refer to companion paper Ref. 26), which provided us with additional means to assign them to specific bands as predicted by the calculations. For anthracene and tetracene, the bands were not resolved enough to determine reliably the symmetries. Line positions and relative intensities of the experimental and theoretical spectra are given as an indication between the best matches; also listed are the theoretically computed symmetries, major resonance components, and intensity sources for each peak or feature. The major resonance components are determined as the fundamentals/combination-bands whose contributions dominate the polyad, as evaluated from the eigenvector component. The "sources" of IR intensities listed are the vibrational fundamentals that lend the most intensity through resonance to each band. Note that the major vibrational resonance components are not necessarily the major intensity sources and vice versa. In some cases, there is more than one dominant resonance component, with nearly equal contributions of various fundamentals or combination modes. Labeling of a given band with a single fundamental or combination state can thus be ambiguous.

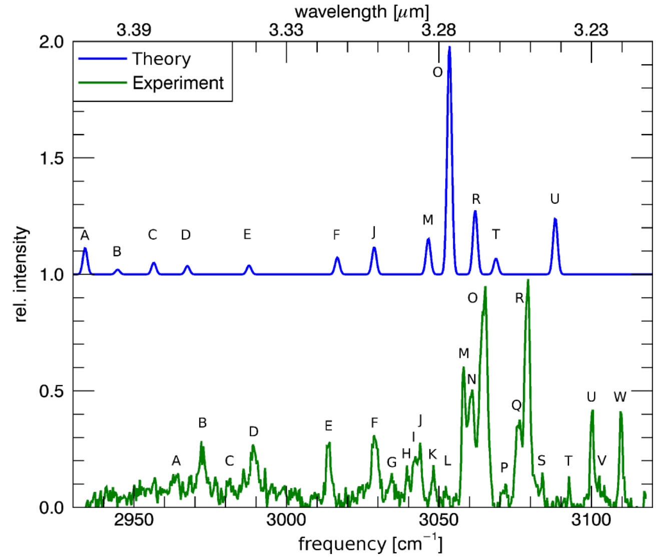

FIG. 5. Anharmonic QFF IR spectrum of naphthalene (this work) compared to high-resolution gas-phase IR absorption spectra obtained in a molecular beam (this work).

V. DISCUSSION

A. Full infrared range

The theoretical anharmonic spectra of all three molecules for the full IR range (Figures 2–4) show good agreement, both

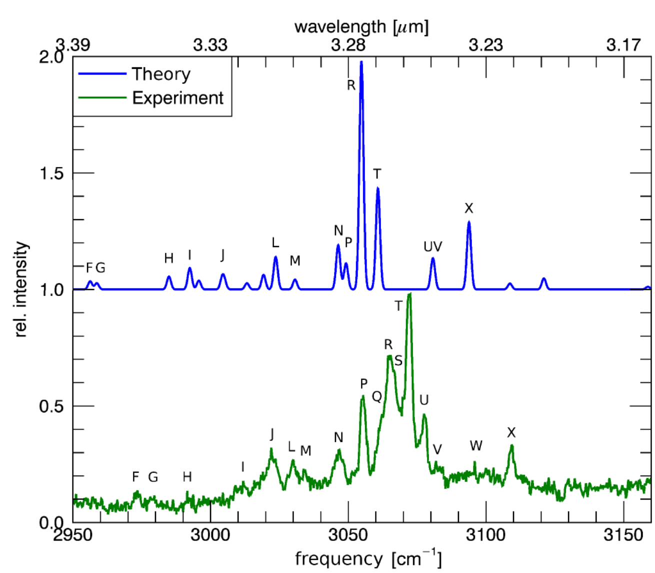

FIG. 6. Anharmonic QFF IR spectrum of anthracene (this work) compared to high-resolution gas-phase IR absorption spectra obtained in a molecular beam (this work).

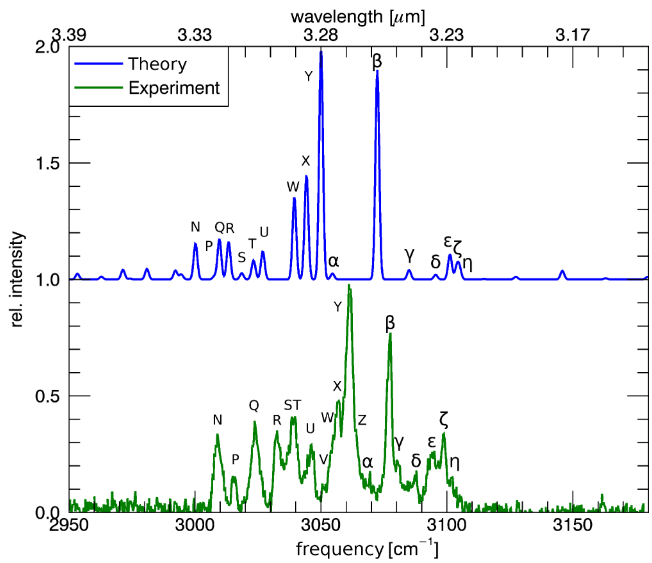

FIG. 7. Anharmonic QFF IR spectrum of tetracene (this work) compared to high-resolution gas-phase IR absorption spectra obtained in a molecular beam (this work).

in band position and relative intensities, with the NIST and matrix-isolation data. Inspection of Tables V–VII shows that the bands in the theoretical anharmonic spectrum differ from experiment by an absolute average deviation for naphthalene of 6.5 cm^{-1} with a maximum deviation of 28 cm^{-1}, for anthracene by an absolute average deviation of 10.2 cm^{-1} with a maximum deviation of 18 cm^{-1}, and for tetracene by an absolute average deviation of 7.4 cm^{-1} with a maximum deviation of 39.8 cm^{-1}. These deviations are not frequency dependent nor are there any trends present; there is near even split between being too high in frequency and too low in frequency for each band. This means that these deviations are most due to the level of electronic structure theory, and not physical effects i.e., temperature shifts or emission versus absorption.

The anharmonic calculations of the CH-stretching region of the full IR spectra also show fairly good agreement with the NIST experiments. The shape of this region (the left and right wings of the main feature, as well as the prominent secondary bumps on the left) can be explained with resonances. However, the secondary bumps are too low in frequency when compared with the experimental data, and in fact these are the largest absolute deviations in the full IR comparison of naphthalene and anthracene. These secondary bumps consist of many lines and as such the position of the convolved feature is highly dependent on the individual features. A detailed analysis is therefore postponed until Section V B. Neglecting these secondary bumps, the absolute average deviation for the two molecules falls to 5.6 cm^{-1} for naphthalene with maximum deviation of 13 cm^{-1}, and 9.9 cm^{-1} for anthracene with a maximum deviation of 18 cm^{-1}.

For tetracene, the maximum deviation is due to the line labeled "z." This line was identified in Ref. 11. However, it is right next to the water contamination so possibly the feature is overly intense causing confusion in the assignment with our theoretical data. If this line is neglected, the absolute average deviation falls to 6.4 cm^{-1} with a maximum deviation of 20 cm^{-1}.

It is important to note that these deviations are significantly smaller than the large deviations for the harmonic approximation. Harmonic calculations led to PAH spectra with blue-shifts appearing as a function of state energies (i.e., there is a systematic percentage error). At lower frequencies, the harmonic spectrum tends to differ by 10 cm^{-1} while at the higher frequencies, the spectrum tends to differ by 100 cm^{-1}. This trend in the harmonic spectra of the three

TABLE V. Line positions (cm^{-1}), relative intensities, dominant resonant components, and origin of intensities for the bands of the naphthalene in the high-resolution gas-phase IR absorption spectra obtained in a molecular beam (this work) and the theoretical anharmonic spectrum (this work) as shown in Figure 5.

ID	sym	exp[26]	rel. I[26]	anharm	rel. I	Components	I source
A	b_{1u}	2963.8	0.20	2934.0	0.12	$\nu_{15}+\nu_{11}$	ν_3
						$\nu_{14}+\nu_{12}$	
B	b_{1u}	2972.4	0.30	2944.6	0.021	ν_7	ν_3
						$\nu_{15}+\nu_{11}$	ν_7
						$\nu_{16}+\nu_{10}$	
C	b_{2u}	2981.3	0.20	2956.4	0.032	ν_2	ν_2
						ν_6	
						$\nu_{13}+\nu_{12}$	
C	b_{1u}	2981.3	0.20	2956.6	0.020	$\nu_{14}+\nu_{12}$	ν_3
						$\nu_{16}+\nu_{10}$	
D	b_{1u}	2989.0	0.28	2967.5	0.037	ν_3	ν_3
						ν_7	
						$\nu_{17}+\nu_9$	
E	b_{2u}	3014.0	0.30	2987.7	0.039	ν_6	ν_2
						$\nu_{15}+\nu_9$	
F	b_{1u}	3029.5	0.19	3016.6	0.074	ν_7	ν_7
						$\nu_{13}+\nu_{11}$	
G	…	3034.5	0.15	…	…	…	…
H	…	3039.5	0.19	…	…	…	…
I	…	3042.3	0.29	…	…	…	…
J	b_{2u}	3043.8	0.35	3028.8	0.12	ν_2	ν_2
						ν_6	
						$\nu_{14}+\nu_{10}$	
						$\nu_{15}+\nu_9$	
K	…	3048.2	0.19	…	…	…	…
L	…	3052.2	0.17	…	…	…	…
M	b_{2u}	3058.1	0.65	3046.5	0.16	ν_2	ν_2
						ν_6	
						$\nu_{14}+\nu_{10}$	
N	…	3060.5	0.54	…	…	…	…
O	b_{1u}	3065.2	0.99	3053.4	1	ν_3	ν_3
P	…	3071.4	0.10	…	…	…	…
Q	…	3076.2	0.37	…	…	…	…
R	b_{2u}	3079.2	1	3061.9	0.28	ν_2	ν_2
						$\nu_{12}+\nu_{11}$	
						$\nu_{14}+\nu_{10}$	
S	…	3092.6	0.21	…	…	…	…
T	b_{1u}	3083.9	0.16	3068.7	0.069	ν_7	ν_3
						$\nu_{13}+\nu_{10}$	ν_7
U	b_{2u}	3100.2	0.45	3088.1	0.24	ν_2	ν_2
						$\nu_{12}+\nu_{11}$	
V	…	3102.6	0.21	…	…	…	…
W	…	3109.4	0.45	…	…	…	…

TABLE VI. Line positions (cm^{-1}), relative intensities, dominant resonant components, and origin of intensities for the bands of anthracene in the high-resolution gas-phase IR absorption spectra obtained in a molecular beam (this work) and the theoretical anharmonic spectrum (this work) as shown in Figure 6.

ID	sym	exp[26]	rel. I[26]	anharm	rel. I	Components	I source
F	b_{1u}	2973.2	0.10	2956.2	0.036	$\nu_{21}+\nu_{13}$	ν_3
						$\nu_{22}+\nu_{12}$	
G	b_{1u}	2979.6	0.08	2958.6	0.028	$\nu_{21}+\nu_{13}$	ν_3
						$\nu_{22}+\nu_{12}$	ν_{10}
H	b_{2u}	2992.5	0.07	2984.8	0.056	ν_6	ν_2
						$\nu_{18}+\nu_{14}$	
						$\nu_{20}+\nu_{11}$	
I	b_{1u}	3011.8	0.15	2992.4	0.094	ν_3	ν_7
						$\nu_{17}+\nu_{14}$	
J	b_{1u}	3022.0	0.30	3004.2	0.050	$\nu_{17}+\nu_{14}$	ν_3
						$\nu_{19}+\nu_{11}$	
						$\nu_{21}+\nu_{12}$	
J	b_{2u}	3022.0	0.30	3005.0	0.027	$\nu_{17}+\nu_{14}$	ν_3
						$\nu_{19}+\nu_{11}$	
						$\nu_{21}+\nu_{12}$	
L	b_{1u}	3030.0	0.25	3023.6	0.14	ν_{10}	ν_{10}
						$\nu_{18}+\nu_{13}$	
M	b_{2u}	3033.7	0.20	3030.6	0.043	$\nu_{17}+\nu_{13}$	ν_2
N	b_{2u}	3046.7	0.30	3046.3	0.19	ν_2	ν_2
						ν_6	
P	b_{1u}	3055.4	0.54	3049.1	0.11	ν_7	ν_7
						$\nu_{18}+\nu_{13}$	
Q	…	3062.3	0.45	…	…	…	…
R	b_{1u}	3065.3	0.72	3054.7	1	ν_3	ν_3
S	…	3066.9	0.64	…	…	…	…
T	b_{2u}	3071.9	1	3060.7	0.44	ν_2	ν_2
						$\nu_{15}+\nu_{14}$	
						$\nu_{17}+\nu_{12}$	
						$\nu_{17}+\nu_{13}$	
U	b_{2u}	3077.8	0.40	3080.5	0.052	$\nu_{17}+\nu_{12}$	ν_2
V	b_{1u}	3081.8	0.24	3080.8	0.088	$\nu_{18}+\nu_{12}$	ν_3
W	…	3095.9	0.24	…	…	…	…
X	b_{2u}	3109.6	0.32	3093.8	0.29	ν_2	ν_2
						$\nu_{15}+\nu_{14}$	

TABLE VII. Line positions (cm^{-1}), relative intensities, dominant resonant components, and origin of intensities for the bands of tetracene in the high-resolution gas-phase IR absorption spectra obtained in a molecular beam (this work) and the theoretical anharmonic spectrum (this work) as shown in Figure 7.

ID	sym	exp[26]	rel. I[26]	anharm	rel. I	Components	I source
N	b_{1u}	3008.9	0.39	3000.0	0.16	ν_7	ν_3
						$\nu_{21}+\nu_{16}$	ν_7
						$\nu_{23}+\nu_{14}$	
P	b_{2u}	3015.3	0.20	3007.7	0.013	$\nu_{20}+\nu_{18}$	ν_2
						$\nu_{25}+\nu_{14}$	
Q	b_{1u}	3023.7	0.44	3009.6	0.17	ν_7	ν_3
						$\nu_{21}+\nu_{16}$	ν_7
						$\nu_{23}+\nu_{14}$	ν_{10}
R	b_{1u}	3032.6	0.40	3013.2	0.17	ν_{10}	ν_{10}
						$\nu_{23}+\nu_{14}$	
S	b_{2u}	3038.5	0.45	3018.6	0.034	$\nu_{22}+\nu_{16}$	ν_2
T	b_{1u}	3039.7	0.46	3022.8	0.023	$\nu_{19}+\nu_{17}$	ν_2
							ν_{11}
T	b_{1u}	3039.7	0.46	3023.4	0.063	$\nu_{26}+\nu_{13}$	ν_3
U	b_{1u}	3046.2	0.34	3026.9	0.12	$\nu_{24}+\nu_{13}$	ν_3
V	…	3050.6	0.18	…	…	…	…
W	b_{1u}	3054.8	0.38	3039.4	0.35	ν_7	ν_7
						ν_{10}	ν_{10}
						$\nu_{21}+\nu_{16}$	
X	b_{2u}	3056.8	0.51	3043.9	0.15	ν_{11}	ν_2
						$\nu_{19}+\nu_{17}$	
X	b_{2u}	3056.8	0.51	3044.3	0.31	ν_2	ν_2
						ν_6	
						$\nu_{18}+\nu_{17}$	
Y	b_{1u}	3061.1	1	3050.0	1	ν_3	ν_3
Z	…	3066.6	0.20	…	…	…	…
α	b_{2u}	3069.5	0.23	3054.6	0.025	ν_6	ν_6
						$\nu_{18}+\nu_{17}$	
β	b_{2u}	3077.6	0.80	3072.3	0.90	ν_2	ν_2
γ	b_{1u}	3080.4	0.27	3085.0	0.041	$\nu_{19}+\nu_{16}$	ν_3
							ν_{10}
δ	b_{1u}	3087.9	0.23	3095.5	0.020	$\nu_{20}+\nu_{14}$	ν_7
ϵ	b_{1u}	3094.1	0.31	3101.0	0.11	$\nu_{18}+\nu_{16}$	ν_3
ζ	b_{2u}	3098.8	0.38	3103.9	0.048	$\nu_{22}+\nu_{13}$	ν_2
η	b_{1u}	3101.5	0.19	3104.9	0.040	$\nu_{18}+\nu_{16}$	ν_7
						$\nu_{21}+\nu_{13}$	ν_{10}

PAHs studied is consistent with the frequency scaling factor of 0.958 that is typically used in the literature[23] to bring the harmonic spectra into closer agreement with matrix-solation experiments.

The experimental and theoretical intensities are normalized to each of their strongest intensities in order to compare their relative intensities. The average relative intensity ratios for the theoretical spectra to the experimental spectra for naphthalene, anthracene, and tetracene are 0.92, 1.01, and 1.41, respectively. These are in excellent agreement, but it is unclear if, in the case of tetracene, matrix interactions are the cause for some of the experimental lines to be lower in intensity when compared to theory.

The NIST/MIS experimental spectra of the three PAHs show a large number of bands in the 1200–2600 cm^{-1} range with intensities comparable to the fundamental bands in the same region. These have been previously attributed, both experimentally[45,46] and theoretically,[47] to combination-bands, although at that time it was only possible to calculate their frequencies and not their intensities. We now can confirm that these bands are indeed pure combination–bands possessing their own unborrowed (non-resonant) anharmonic intensities. These combination–bands show good enough agreement with experimental results that a more detailed set of line assignments would be possible if higher resolution experimental spectra were to be taken in this region. It was found that the VPT2 is capable of reliable predictions without the aid of polyad mixings for this wavelength range. These combination bands are found to be generated by modes of the same type, i.e., out–of–plane in combination with out–of–plane, and in–plane in combination with in–plane. The out-of-plane–out-of-plane combination bands range from 1200–1900 cm^{-1} and the in-plane–in-plane combination bands range from

2200–2600 cm^{-1}. The out-of-plane–out-of-plane combination bands are found to have more intensity than the in-plane–inplane combination bands by approximately an order of magnitude. Bands originating between a combination of one in–plane mode and one out–of–plane mode were not found to have significant intensity, even in other frequency regions.

B. CH–stretching region

Our high–resolution gas–phase experiments allow for a closer look at the effect of resonances in the CH–stretching region of PAH spectra. Indeed, the large number of CH–stretching bands in the experimental spectra shown in Figures 5–7 (naphthalene, anthracene, and tetracene respectively) cannot be explained by the harmonic approximation.

Line positions for naphthalene, anthracene, and tetracene differ between our anharmonic calculations and our experimental spectra by absolute deviations of 19.3 cm^{-1}, 10.5 cm^{-1}, and 11.7 cm^{-1}, with maximum absolute deviations of 29.8 cm^{-1}, 21.0 cm^{-1}, and 19.9 cm^{-1} respectively. All theoretical frequencies were left unscaled.

The three molecules in this study belong to the D_{2h} point group for which only type–two Fermi resonances ($\nu_i \approx \nu_j + \nu_k$) are of importance for the analysis of the spectrum. Type–one Fermi resonances ($\nu_i \approx 2\nu_j$) have no effect since for this point group, all overtones are totally symmetric and hence not IR active. The IR–active modes belong to b_{1u}, b_{2u}, and b_{3u} symmetries. However, the b_{3u} symmetry modes are out–of–plane modes and therefore the fundamental and combination bands do not occur in the CH–stretching region. This means that the CH–stretching region is mainly controlled by two large vibrational resonance polyads, one for the b_{1u} symmetry bands and the other one for the b_{2u} symmetry bands. These large polyads have a significant effect on the resulting spectrum and completely change the band positions and intensities when moving from the harmonic to the non-polyad VPT2 and to the polyad VPT2 anharmonic simulation.[26]

It has been shown in this work that the anharmonic QFF treatment can reproduce the large number of bands seen in the CH–stretching region for anthracene and tetracene. Our experiment for naphthalene, however, shows many more lines than can be explained with the current "VPT2 + resonance polyad" approach. In previous experiments, it could not be ruled out that some (or more) of these bands were actually due to isotopologues or other contaminations, or associated with excitation from vibrationally excited levels. The mass-resolved and conformer selectivity nature of our experiments and the use of supersonically cooled molecules ensure that in our experiments, we can unambiguously conclude that all of the measured CH-stretching features concern excitations from the vibrational ground state of each PAH, even though our current theory cannot explain all of them adequately. One possible explanation for the presence of additional bands is that the resonance polyads should include second overtones or combination–bands of three (or more) vibrational quanta or modes to explain all the observed experimental lines.

Though subtle, there seems to be a slight effect in the spectral range over which features are observed in the CH-stretching region when comparing the three experimental spectra (Figs. 2–4). The spectral range narrows when PAH length increases. This may be explained by the linear increase of the number of CH oscillators with increasing length of the PAH together with the vibrational state density increasing much more rapidly. Since one can reasonably assume that the anharmonic coupling strengths are not significantly influenced by the size of the PAH, the available oscillator strength, increasing roughly linearly with PAH size, will be distributed over many more background levels. Since the intensity borrowing is roughly inversely proportional with the distance to the fundamental band, this effectively leads to a narrowing of the CH-stretching band envelope. Such a conclusion is further supported by MIS studies on larger PAHs,[11] which indeed show that the spectral band envelope becomes increasingly narrower for larger PAHs.

It can be seen that the frequencies of the major CH-stretching fundamental bands are about the same for all types of PAHs. The frequencies of the CC stretching modes that are potentially involved in combination-bands, on the other hand, are much more sensitive to the finer structure details and point group of the individual PAH. Consequently, from species to species, the minor CH-stretching region bands vary vastly more than predicted by the harmonic level analysis. This dramatic effect on the overall CH-stretching region can aid in the identification of specific species or sub-families of PAHs.

The average relative intensities ratios for the theoretical spectra to the experimental spectra for naphthalene, anthracene, and tetracene are 0.34, 0.48, and 0.36 respectively. The theoretical spectra are normalized to the strongest bands, which for naphthalene is the band labeled "O," for anthracene is the band labeled "R," and for tetracene are the two nearly equal bands "Y" and "β." This however leaves the remaining intensities under scaled. This is especially obvious for the second strongest band of naphthalene, "R" and the second strongest band of anthracene, "T." If these strongest intensities are ignored and the spectra are instead normalized to the remaining bands, the average ratio between theory to experiment jumps to 1.01, 0.95, and 0.93 for naphthalene, anthracene, and tetracene respectively. This leads us to believe that there may be either an issue with the double harmonic intensity calculations of the strongest CH-stretching fundamental bands, possibly due to the level of electronic structure theory used (as happens with the overestimation of the C–H stretching intensities for the B3LYP/4-31G case[23]), or the triple-combination-band resonances borrow significant intensity from the strongest bands. We are presently investigating this issue in more detail.

C. Astrophysical implications

Our study demonstrates that anharmonicity needs to be taken into account in order to have a more reliable understanding of astronomical IR PAH spectra. Current astronomical observations and modelling of the AIBs rely exclusively on the harmonic IR spectrum of PAHs, which fail to reproduce the spectra in a number of ways.

The shape and strength of all of the features falling in the C–H stretching region are controlled by resonances and anharmonicity; thus, the harmonic approximation utterly fails here. Astronomical spectra of AIBs indeed show a series of secondary features, such as wings and broad plateaux close to the main 3.29 μm (3030 cm^{-1}) feature, which so far have not been adequately characterized.[48] Anharmonic studies of PAHs can help shed light on the origin of these features and possibly their dependence on the structural properties of PAHs.[26] PAHs of varying shapes will be investigated in future work.

Current harmonic models do not predict any bands in the 5–5.5 μm region (2000–1820 cm^{-1}), although observations of the AIBs do see emission in this region.[47] The anharmonic calculations of this work have confirmed that these observed bands are indeed due to PAHs, specifically combination bands with their own relatively strong intrinsic intensities.

Astronomical emission models of PAHs rely on the so-called "infrared cascade,"[48] e.g., the energy of a photon is distributed amongst the harmonic IR active modes of the absorbing PAH. Since, in a real molecule, many more states are IR active due to anharmonicity, the energy distribution and therefore the resulting emission spectra of PAHs will lead to spectral complexity that may actually aid in species identification and understanding of astronomical PAHs. Inclusion of anharmonicity also allows for the inclusion of hot bands and overtones into models[20,49,50] and will be investigated in future work.

Fianlly, anharmonic calculations eliminate the need for the typical frequency scaling factor[23] that is used to bring harmonic theoretical spectra into agreement with experimental matrix-isolation spectra. No frequency scaling factors or shifts are found in this work, and line positions are accurately determined to within 10 cm^{-1}, with no bias towards either a red or blue shifts. Investigation into the possible causes of this error, i.e., the level of theory, is underway and will be reported in due course. Bearing this, anharmonic calculations do provide greater confidence in the theoretical spectra, especially when extrapolating to areas where experimental data are limited.

VI. CONCLUSIONS

In this work, we calculated the anharmonic IR spectrum of naphthalene, anthracene, and tetracene, (the last two for the first time) and compare them with available gas-phase and MIS experiments, as well as our own low-temperature high-resolution gas-phase spectra in the CH–stretching region. It has been shown that there are clear differences between a harmonic IR spectrum and an anharmonic IR spectrum. Theoretical anharmonic spectra are needed in order to explain combination-bands, resonances in the C–H stretching region, as well as the frequency shifting factor normally seen in harmonic spectra simulation. Our anharmonic theoretical spectra are in excellent agreement with the experimental spectra.

All of the fundamental CH–stretching modes for each of the PAHs studied are in resonance with many combination-bands. This occurs because PAHs have a large number of CC-stretching modes around 1500 cm^{-1} that can enter into type-two Fermi resonances ($\nu_i \approx \nu_j + \nu_k$) with the CH-stretching modes around 3000 cm^{-1}. This type of resonance explains the asymmetric wings and overall shape observed in the CH region in low resolution experiments, and the large number of lines found in our high-resolution experiments. However, the comparison between predicted and experimentally observed spectra also indicates that there are still lines that cannot be accounted for. It is possible that this is due to potential interactions that were not accounted for such as combination-bands or higher order overtone states involving three or more vibrational quanta or modes. We can conclude that without the intensity borrowing between resonant states, the number of computed features with significant intensity is unable to match the experiment. Sharing intensities through resonances produces spectra that better match the general shape and features in the CH stretch region when compared to harmonic treatments or VPT2 treatments that neglect intensity sharing and polyad resonances.[26]

The 1700–2500 cm^{-1} spectral region is also unaccounted for in the harmonic approximation but shows up in experimental data. Experimental spectra show bands with noticeable intensity in this region, sometimes as strong as, or even greater than the surrounding fundamental bands. These bands are found to be combination-bands and can be predicted very well by the VPT2 anharmonic analysis both with respect to position and intensity. Since these bands are not involved in resonances, VPT2 reliably predicts these lines without the aid of polyad mixing.

In this work, deviations in band positions and intensity problems in the CH-stretching region have been partially attributed to the level of electronic structure theory. Due to the size of the molecules studied in this work, current computational resources limit the level of theory that can be used. However, naphthalene QFF analysis is just barely feasible for the CCSD(T) approach with cc-pVTZ basis. A detailed analysis into the effects of the level of electronic structure theory on anharmonic calculations of PAHs is currently underway using naphthalene as the test case.

The spectra comparison among the three PAHs studied in this work suggests that our anharmonic treatment may perform better as the size of the PAHs increases. Additional experimental and theoretical work on larger PAHs is currently underway using the same theoretical and experimental approaches as described in this work. Furthermore, it is hoped that better understanding of the effects that vibrational anharmonicities have on a typical PAH spectrum can possibly lead to more general predictions of the PAH family as a whole without the need for detailed anharmonic analyses on all PAH molecules.

ACKNOWLEDGMENTS

The authors would like to thank the two anonymous reviewers for their helpful comments that improved the clarity of the manuscript. The spectroscopic study of interstellar PAHs at Leiden Observatory has been supported through the Advanced European Research Council Grant No. 246976, a Spinoza award, and through the Dutch Astrochemistry Network funded by the Netherlands Organization for Scientific Research, NWO. Computing time has been made available by NWO Exacte Wetenschappen (Project Nos. MP–270–13 and MP–264–14) and calculations were performed at the LISA Linux cluster of the SurfSARA supercomputer center in Almere, The Netherlands. X.H. and T.J.L. gratefully acknowledge support from the NASA No. 12–APRA12–0107 grant. X.H. acknowledges the support from NASA/SETI Co–op Agreement Nos. NNX12AG96A and NNX15AF45A. This material is based upon work supported by the National Aeronautics and Space Administration through the NASA Astrobiology Institute under Cooperative Agreement Notice No. NNH13ZDA017C issued through the Science Mission Directorate. A.C. acknowledges Fernando Clemente and Julien Bloino for insightful discussions.

APPENDIX: MODE DESCRIPTIONS

TABLE VIII. Mode descriptions and harmonic frequencies (cm^{-1}) of all IR active modes with double harmonic intensities >0.05 km/mol and all modes that are involved in active combinations identified in this work for naphthalene. OP—out of plane; IP—in plane; LS—long side; TS—terminal side (see Fig. 1); MR—middle ring; TR – terminal ring (see Fig. 1); || perpendicular to ring-ring-ring axis; = parallel to ring-ring-ring axis.

Mode	Freq	Symm	Description
ν_2	3184.55	b_{2u}	asym TS sym str (IP) || a =s
ν_3	3172.85	b_{1u}	sym TS-LS asym str (IP) || s =a
ν_6	3157.92	b_{2u}	asym TS-LS CH sym IP str || a =s
ν_7	3155.20	b_{1u}	sym LS+TS asym str (IP) || s =a
ν_9	1661.12	b_{3g}	sym 2-ring CH rock || a =a
ν_{10}	1631.73	b_{1u}	sym CC and CH rock/wag (IP) || s =a
ν_{12}	1542.43	b_{2u}	asym CC and CH wag, boating (IP) || a =s
ν_{13}	1487.71	a_g	sym 2-ring CH sym wag || s =s
ν_{14}	1485.75	b_{3g}	asym 2-ring CH rock || a =a
ν_{15}	1415.55	b_{1u}	sym ring CH rotation (sym rock) (IP) || s =a
ν_{16}	1393.46	a_g	center CC str || s =s
ν_{17}	1386.34	b_{2u}	asym CC and CH wag, (IP) || a =s
ν_{18}	1283.93	b_{1u}	sym LS rock (IP) || s =a
ν_{20}	1227.77	b_{2u}	asym TS wag (IP) || a =s
ν_{23}	1163.89	b_{2u}	asym CH wag (IP) || a =s
ν_{24}	1147.15	b_{1u}	sym CH rock/wag (IP) || s =a
ν_{26}	1030.13	b_{2u}	asym 2-ring breath (IP) || a =s
ν_{27}	996.25	b_{2g}	sym TS asym OP bend || s =a
ν_{28}	990.94	a_u	asym TS asym OP bend || a =a
ν_{29}	979.34	b_{3u}	sym LS sym OP bend, || s =s
ν_{32}	894.74	b_{2g}	sym CH asym OP bend || s =a
ν_{33}	846.53	a_u	asym CH asym OP bend || a =a
ν_{34}	804.60	b_{1u}	sym TS asym CC IP deform || s =a
ν_{35}	797.02	b_{3u}	sym CH sym OP bend (CH inversion) || s =s
ν_{36}	783.13	b_{2g}	asym LS sym OP bend || s =a
ν_{38}	725.96	b_{1g}	asym CH sym OP bend (CH invers) || a =s
ν_{40}	629.79	b_{2u}	2-ring asym str (IP) || a =s
ν_{43}	482.17	b_{3u}	sym MR CH sym OP bend, fly || s =a
ν_{46}	362.72	b_{1u}	2-ring ip bend || s =a
ν_{47}	183.92	a_u	2-ring torsion OP || a =a
ν_{48}	170.25	b_{3u}	2-ring OP bend || s =s

TABLE IX. Mode descriptions and harmonic frequencies (cm^{-1}) of all IR active modes with double harmonic intensities >0.05 km/mol and all modes that are involved in active combinations identified in this work for anthracene. OP—out of plane; IP – in plane; LS—long side; TS—terminal side (see Fig. 1); MR – middle ring; TR—terminal ring (see Fig. 1); || perpendicular to ring–ring–ring axis; = parallel to ring-ring-ring axis.

Mode	Freq	Symm	Description
ν_2	3185.13	b_{2u}	asym TR CH sym str (IP) || a =s
ν_3	3173.31	b_{1u}	sym TR asym CH str (IP) || s =a
ν_6	3159.62	b_{2u}	asym (LS-TR + TS) CH IP sym str || a =s
ν_7	3155.52	b_{1u}	sym LS asym str, TS asym str (IP) || s =a
ν_{10}	3150.78	b_{1u}	MR CH asym str (IP) || s =a
ν_{11}	1660.53	b_{1u}	sym 3-ring CC, CH rock/wag (IP) || s =a
ν_{12}	1658.31	b_{3g}	sym 3-ring CH rock || a =a
ν_{13}	1614.96	b_{3g}	asym 3-ring CC, CH rock/wag (IP) || s =a
ν_{14}	1587.51	a_g	4-center-CC sym str, CH wag (IP) || s =s
ν_{15}	1571.72	b_{2u}	asym 3-ring CC, CH wag (IP) || a =s
ν_{17}	1480.78	b_{1u}	TS ring CH sym rock (rotation) (IP)|| s =a
ν_{18}	1478.96	b_{2u}	asym TR CH wag (IP) || a =s
ν_{19}	1422.09	a_g	4-center-CC asym str (IP) || s =s
ν_{20}	1411.80	b_{3g}	asym TR CH rock (rotation) (IP) || a =a
ν_{21}	1410.82	b_{2u}	MR asym CC + CH wag (IP) || a =s
ν_{22}	1371.66	b_{2u}	sym LS wag (boating) (IP) || a =s
ν_{23}	1333.61	b_{1u}	sym TR CH rock (IP) || s =a
ν_{24}	1291.48	b_{3g}	MR CH rock (IP) || a =a
ν_{25}	1287.35	b_{1u}	sym TS ring LS asym CH rock (IP) || s =a
ν_{27}	1206.72	b_{3g}	sym LS rock (IP) || a =a
ν_{28}	1186.78	a_g	sym TR CH asym wag (IP) || a =a
ν_{29}	1185.52	b_{2u}	asym TS rock, MR CH rock (IP)
ν_{31}	1152.89	b_{2u}	3-ring sym CH wag (boating) (IP) || a =s
ν_{34}	1020.99	b_{2u}	asym TR breath (IP) || a =s
ν_{35}	991.76	b_{2g}	sym TR CH asym OP bend || s =a
ν_{36}	991.45	a_u	asym TR CH asym OP bend || a =a
ν_{37}	976.83	b_{3u}	sym LS bend - sym TS bend (OP) || s =s
ν_{38}	971.95	b_{1g}	asym TR CH asym OP bend || a =s
ν_{39}	926.06	b_{3g}	asym 3-ring deformation (IP) || a =a
ν_{40}	916.28	b_{1u}	sym 3-ring distorsion (IP) || s =a
ν_{41}	911.17	b_{2g}	MR CH - TR CH asym bend (OP) || s =a
ν_{42}	898.87	b_{3u}	MR CH sym OP bend (inversion) || s =s
ν_{43}	864.31	a_u	asym TR CH OP torsional bend || a =a
ν_{44}	842.26	b_{2g}	MR CH - TR CH asym bend (OP) || s =a
ν_{45}	817.11	b_{2u}	3-ring MR IP swing || a =s
ν_{46}	781.16	b_{2g}	sym 3-ring LS asym OP bend || s =a
ν_{47}	768.17	b_{1g}	asym TR CH sym OP bend || a =s
ν_{49}	755.09	a_u	asym 3-ring OP bend || a =a
ν_{50}	738.36	b_{3u}	sym TS sym OP bend (inversion) || s =s
ν_{51}	657.68	b_{1u}	sym 3-ring wag (IP) || s =a
ν_{53}	612.64	b_{2u}	asym TS ring str (IP) || a =s
ν_{57}	480.17	b_{1g}	asym TR LS sym OP bend || a =s
ν_{58}	473.60	b_{3u}	LS 3-ring inversion, fly (OP) || s =s
ν_{59}	395.96	a_g	sym 3-ring stretch || s =s
ν_{61}	384.15	b_{3u}	3-ring TR OP folding || s =s
ν_{63}	234.35	b_{1u}	3-ring linear bend (IP) || s =a
ν_{66}	89.25	b_{3u}	3-ring linear bend (OP) || s =s

TABLE X. Mode descriptions and harmonic frequencies (cm^{-1}) of all IR active modes with double harmonic intensities >0.05 km/mol and all modes that are involved in active combinations identified in this work for tetracene. OP—out of plane; IP—in plane; LS—long side; TS—terminal side (see Fig. 1); MR—middle ring; TR—terminal ring (see Fig. 1); || perpendicular to ring-ring-ring axis; = parallel to ring-ring-ring axis.

Mode	Freq	Symm	Description
ν_2	3185.35	b_{2u}	asym TR CH sym str (IP) || a =s
ν_3	3173.56	b_{1u}	sym TR CH asym str (IP) || s =a
ν_6	3160.07	b_{2u}	asym TR CH sym str (IP) || a =s
ν_7	3155.71	b_{1u}	sym LS asym str (IP) || s =a
ν_{10}	3153.01	b_{1u}	sym MR CH sym str (IP) || s =a
ν_{11}	3152.32	b_{2u}	asym MR CH sym str (IP) || a =s
ν_{13}	1666.71	b_{1u}	sym 4-ring CH rock (IP) || s =a
ν_{14}	1652.99	b_{3g}	asym TR CH wag/rock (IP) || a =a
ν_{16}	1598.83	b_{1u}	sym 4-ring distorsion (IP) || s =a
ν_{17}	1575.65	b_{2u}	asym 4-ring distorsion (IP) || a =s
ν_{18}	1571.66	a_g	5-center-CC sym str, TS wag || s =s
ν_{19}	1549.92	a_g	asym center CC str, CH rock/wag || s =s
ν_{20}	1497.03	b_{2u}	asym TR CH wag (IP) || a =s
ν_{21}	1476.24	a_g	sym TR CH sym wag (IP) || s =s
ν_{22}	1474.48	b_{3g}	asym TR CH sym rock (IP) || a =a
ν_{23}	1426.85	b_{2u}	asym 4-ring distorsion (IP) || a =s
ν_{24}	1420.27	a_g	sym MR CH wag (IP) || s =s
ν_{25}	1415.01	b_{1u}	sym TR rotation (IP) || s =a
ν_{27}	1363.63	b_{2u}	sym LS wag (IP) boating mode || a =s
ν_{29}	1311.03	b_{1u}	sym MR distorsion + CH rock (IP) || s =a
ν_{30}	1310.82	b_{2u}	asym MR breath (IP) || a =s
ν_{31}	1295.33	b_{1u}	sym MR CH rock (IP) || s =a
ν_{34}	1218.47	b_{1u}	asym LS rock (IP) || s =a
ν_{35}	1200.03	b_{3g}	sym LS asym rock (IP) || a =a
ν_{36}	1185.82	b_{2u}	asym TR CH wag || a =s
ν_{39}	1144.78	b_{1u}	sym TS rock (IP) || s =a
ν_{40}	1140.55	b_{2u}	sym LS rock (IP) || a =s
ν_{42}	1015.03	b_{2u}	asym TR CH wag (IP) || a =s
ν_{43}	990.72	b_{2g}	sym TR CH asym OP bends || s =a
ν_{44}	990.64	a_u	asym TR CH asym OP bends || a =a
ν_{45}	976.59	b_{3u}	TR CH asym OP bend, fly || s =s
ν_{46}	975.23	b_{1g}	asym TR CH asym OP bends || a =s
ν_{47}	942.45	b_{1u}	4-ring distorsion (IP) || s =a
ν_{48}	918.32	b_{3u}	sym MR CH sym OP bend || s =s
ν_{49}	914.96	b_{2g}	sym MR CH asym OP bends || s =a
ν_{51}	887.84	a_u	asym 2-ring 2-ring CH OP bend || a =a
ν_{52}	865.37	b_{1g}	asym MR CH sym OP bends || a =s
ν_{54}	851.11	b_{2g}	sym 4-ring CH asym OP bends || s =a
ν_{55}	839.45	a_u	asym 4-ring CH asym OP bends || a =a
ν_{57}	777.54	b_{2g}	sym 4-ring LS asym OP bends || s =a
ν_{60}	755.83	b_{3u}	sym TR CH sym OP bend || s =a
ν_{61}	754.29	b_{2u}	asym 4-ring breath (IP) || a =s
ν_{62}	742.15	b_{1g}	asym TR CH sym OP bend || a =s
ν_{63}	730.33	b_{2g}	asym 4-ring OP bend || a =a
ν_{64}	638.61	b_{2u}	4-ring asym str (IP) || a =s
ν_{66}	613.82	b_{1u}	4-ring distorsion (IP) || s =a
ν_{68}	558.68	b_{2u}	4-ring asym str (IP) || a =s
ν_{71}	478.92	b_{3u}	LS asym OP bend, fly || s =s
ν_{73}	467.72	b_{3u}	LS sym OP bend || s =s
ν_{74}	443.83	b_{1u}	sym ring-ring IP bending || s =a
ν_{77}	314.06	a_u	asym 4-ring torsion || a =a
ν_{79}	267.98	b_{3u}	4-ring waving (OP) || s =s
ν_{81}	162.33	b_{1u}	4-ring linear bend (IP) || s =a
ν_{84}	54.32	b_{3u}	4-ring linear bend (OP) || s =s

[1] H. Lai, M. Lin, M. Yang, and A. Li, Mater. Sci. Eng.: C **16**, 23 (2001).
[2] J. Berashevich and T. Chakraborty, J. Phys. Chem. C **115**, 24666 (2011).
[3] X. Wan, K. Chen, D. Liu, J. Chen, Q. Miao, and J. Xu, Chem. Mater. **24**, 3906 (2012).
[4] IARC, Monogr. Eval. Carcinog. Risks Hum. **100**, 111 (2012).
[5] H. Richter and J. Howard, Prog. Energy Combust. Sci. **26**, 565 (2000).
[6] A. M. Mastral and M. S. Callãn, Environ. Sci. Technol. **34**, 3051 (2000).
[7] A. Leger and J. L. Puget, Astron. Astrophys. **137**, L5 (1984).
[8] L. J. Allamandola, A. G. G. M. Tielens, and J. R. Barker, Astrophys. J., Lett. **290**, L25 (1985).
[9] A. G. G. M. Tielens, Annu. Rev. Astron. Astrophys. **46**, 289 (2008).
[10] D. M. Hudgins, S. A. Sandford, and L. J. Allamandola, "Infrared spectroscopy of matrix isolated PAHs," in *The First Symposium on the Infrared Cirrus and Diffuse Interstellar Clouds*, edited by R. M. Cutri and W. B. Latter, Astronomical Society of the Pacific Conference Series Vol. 58 (Astronomical Society of the Pacific, San Francisco, CA, 1994), p. 283.
[11] D. M. Hudgins and S. A. Sandford, J. Phys. Chem. A **102**, 329 (1998).
[12] See supplementary material at http://dx.doi.org/10.1063/1.4936779 for the full theoretical line list and corresponding polyads of each of the three PAHs.
[13] D. M. Hudgins and L. J. Allamandola, J. Phys. Chem. A **101**, 3472 (1997).
[14] D. M. Hudgins and S. A. Sandford, J. Phys. Chem. A **102**, 344 (1998).
[15] A. L. Mattioda, C. W. Bauschlicher, J. D. Bregman, D. M. Hudgins, L. J. Allamandola, and A. Ricca, Spectrochim. Acta, Part A **130**, 639 (2014).
[16] NIST Mass Spec Data Center, S. E. Stein, director, "Infrared Spectra," in *NIST Chemistry WebBook*, NIST Standard Reference Database Number 69, edited by P. J. Linstrom and W. G. Mallard (National Institute of Standards and Technology, Gaithersburg, MD, 2015).
[17] E. Cané, A. Miani, P. Palmieri, R. Tarroni, and A. Trombetti, Spectrochim. Acta, Part A **53**, 1839 (1997).
[18] E. Cané, A. Miani, P. Palmieri, R. Tarroni, and A. Trombetti, J. Chem. Phys. **106**, 9004 (1997).
[19] C. Joblin, L. D'Hendecourt, A. Leger, and D. Defourneau, Astronaut. Aeronaut. **281**, 923 (1994).
[20] O. Pirali, M. Vervloet, G. Mulas, G. Malloci, and C. Joblin, Phys. Chem. Chem. Phys. **11**, 3443 (2009).
[21] C. Boersma, C. W. Bauschlicher, Jr., A. Ricca, A. L. Mattioda, J. Cami, E. Peeters, F. Sánchez de Armas, G. Puerta Saborido, D. M. Hudgins, and L. J. Allamandola, Astrophys. J. **211**, 8 (2014).
[22] G. Malloci, C. Joblin, and G. Mulas, Chem. Phys. **332**, 353 (2007).
[23] S. R. Langhoff, J. Phys. Chem. **100**, 2819 (1996).
[24] M. J. Frisch, G. W. Trucks, H. B. Schlegel, G. E. Scuseria, M. A. Robb, J. R. Cheeseman, G. Scalmani, V. Barone, B. Mennucci, G. A. Petersson, H. Nakatsuji, M. Caricato, X. Li, H. P. Hratchian, A. F. Izmaylov, J. Bloino, G. Zheng, J. L. Sonnenberg, M. Hada, M. Ehara, K. Toyota, R. Fukuda, J. Hasegawa, M. Ishida, T. Nakajima, Y. Honda, O. Kitao, H. Nakai, T. Vreven, J. A. Montgomery, Jr., J. E. Peralta, F. Ogliaro, M. Bearpark, J. J. Heyd, E. Brothers, K. N. Kudin, V. N. Staroverov, R. Kobayashi, J. Normand, K. Raghavachari, A. Rendell, J. C. Burant, S. S. Iyengar, J. Tomasi, M. Cossi, N. Rega, J. M. Millam, M. Klene, J. E. Knox, J. B. Cross, V. Bakken, C. Adamo, J. Jaramillo, R. Gomperts, R. E. Stratmann, O. Yazyev, A. J. Austin, R. Cammi, C. Pomelli, J. W. Ochterski, R. L. Martin, K. Morokuma, V. G. Zakrzewski, G. A. Voth, P. Salvador, J. J. Dannenberg, S. Dapprich, A. D. Daniels, Ö. Farkas, J. B. Foresman, J. V. Ortiz, J. Cioslowski, and D. J. Fox, GAUSSIAN 09, Revision D.01, Gaussian Inc., Wallingford, CT, 2009.
[25] V. Barone, J. Chem. Phys. **122**, 014108 (2005).
[26] E. Maltseva, A. Petrignani, A. Candian, C. J. Mackie, X. Huang, T. J. Lee, A. G. G. M. Tielens, J. Oomens, and W. J. Buma, Astrophys. J. **814**, 23 (2015).
[27] E. B. Wilson, J. C. Decius, and P. C. Cross, *Molecular Vibrations* (McGraw-Hill, 1955), Vol. 305, p. 616.
[28] A. G. Csaszar, Wiley Interdiscip. Rev.: Comput. Mol. Sci. **2**, 273 (2012).
[29] R. Burcl, N. C. Handy, and S. Carter, Spectrochim. Acta, Part A **59**, 1881 (2003).
[30] J. M. Martin, T. J. Lee, P. R. Taylor, and J.-P. François, J. Chem. Phys. **103**, 2589 (1995).
[31] K. K. Lehmann, Mol. Phys. **66**, 1129 (1989).
[32] K. Yagi, S. Hirata, and K. Hirao, Phys. Chem. Chem. Phys. **10**(13), 1781 (2008).
[33] K. Yagi and H. Otaki, J. Chem. Phys. **140**, 084113 (2014).
[34] J. Bloino and V. Barone, J. Chem. Phys. **136** (2012).
[35] A. Willets, N. C. Handy, W. H. Green, Jr., and D. Jayatilaka, J. Chem. Phys. **94**, 5608 (1990).

[36]J. Vázquez and J. F. Stanton, Mol. Phys. **105**, 101 (2007).
[37]J. F. Gaw, A. Willets, W. H. Green, and N. C. Handy, SPECTRO, version 3.0 (1996).
[38]F. A. Hamprecht, A. J. Cohen, D. J. Tozer, and N. C. Handy, J. Chem. Phys. **109**, 6264 (1998).
[39]T. Dunning *et al.*, J. Chem. Phys. **55**, 716 (1971).
[40]E. Cané, A. Miani, and A. Trombetti, J. Phys. Chem. A **111**, 8218 (2007).
[41]A. D. Boese and J. M. L. Martin, J. Phys. Chem. A **108**, 3085 (2004).
[42]V. Barone, M. Biczysko, and J. Bloino, Phys. Chem. Chem. Phys. **16**, 1759 (2014).
[43]C. J. Mackie, A. Candian, X. Huang, T. J. Lee, and A. G. G. M. Tielens, J. Chem. Phys. **142**, 244107 (2015).
[44]S. Smolarek, A. Vdovin, A. Rijs, C. A. van Walree, M. Z. Zgierski, and W. J. Buma, J. Phys. Chem. A **115**, 9399 (2011).
[45]C. W. Young, R. B. DuVall, and N. Wright, Anal. Chem. **23**, 709 (1951).
[46]G. Socrates, *Infrared and Raman Characteristic Group Frequencies: Tables and Charts* (John Wiley & Sons, 2004).
[47]C. Boersma, A. L. Mattioda, C. W. Bauschlicher, Jr., E. Peeters, A. G. G. M. Tielens, and L. J. Allamandola, Astrophys. J. **690**, 1208 (2009).
[48]L. J. Allamandola, A. G. G. M. Tielens, and J. R. Barker, Astrophys. J. **71**, 733 (1989).
[49]C. Pech, C. Joblin, and P. Boissel, Astronaut. Aeronaut. **388**, 639 (2002).
[50]J. R. Barker, L. J. Allamandola, and A. G. G. M. Tielens, Astrophys. J., Lett. **315**, L61 (1987).